BIOCHEMISTRY
including biophysical chemistry & molecular biology
Article

Biochemistry **2009,** *48,* 7229–7239 7229
DOI: 10.1021/bi900670d

Structure-Dependent Charge Density as a Determinant of Antimicrobial Activity of Peptide Analogues of Defensin[†]

Yang Bai,[‡] Shouping Liu,[§] Ping Jiang,[‡] Lei Zhou,[§,@] Jing Li,[§,@] Charles Tang,[∥] Chandra Verma,[⊥] Yuguang Mu,*[,‡] Roger W. Beuerman,*[,§,@,#] and Konstantin Pervushin*[,‡]

[‡]*School of Biological Sciences, Nanyang Technological University, 60 Nanyang Drive, Singapore 637551,* [§]*Singapore Eye Research Institute, 11 Third Hospital Avenue, #06-00, Singapore 168751,* [∥]*Department of Pathology, Pharmaceutical Microbiology Laboratory, Singapore General Hospital, Singapore 168751,* [⊥]*Bioinformatics Institute (A-STAR), 30 Biopolis Street, #07-01 Matrix, Singapore 138671,* [@]*Department of Ophthalmology, Yong Loo Lin School of Medicine, National University of Singapore, 5 Lower Kent Ridge Road, Singapore 119074, and* [#]*School of Chemical and Biomedical Engineering, Nanyang Technological University, 62 Nanyang Drive, Singapore 637459*

Received April 19, 2009; Revised Manuscript Received June 5, 2009

ABSTRACT: Defensins are small (3−5 kDa) cysteine-rich cationic proteins found in both vertebrates and invertebrates constituting the front line of host innate immunity. Despite intensive research, bactericidal and cytotoxic mechanisms of defensins are still largely unknown. Moreover, we recently demonstrated that small peptides derived from defensins are even more potent bactericidal agents with less toxicity toward host cells. In this paper, structures of three C-terminal (R36−K45) analogues of human β-defensin-3 were studied by ^{1}H NMR spectroscopy and extensive molecular dynamics simulations. Because of indications that these peptides might target the inner bacterial membrane, they were reconstituted in dodecylphosphocholine or dodecylphosphocholine/1-palmitoyl-2-oleoyl-*sn*-glycero-3-[phospho-*rac*-(1-glycerol)] mixed micelles, and lipid bicelles mimicking the phospholipid-constituted bilayer membrane of mammalian and bacterial cells. The results show that the binding affinity and partitioning into the lipid phase and the ability to dimerize and accrete well-defined structures upon interactions with lipid membranes contribute to compactization of positive charges within peptide oligomers. The peptide charge density, mediated by corresponding three-dimensional structures, was found to directly correlate with the antimicrobial activity. These novel observations may provide a new rationale for the design of improved antimicrobial agents.

In recent years, strains of bacteria with resistance to one or more conventional antibiotics have emerged at an alarming rate. An urgency to design new generation antimicrobials with improved properties has developed. One of the promising avenues has been natural cationic peptides, such as tachyplesin, cecropin, melitten, and defensins (*1*). In mammals, at least two distinct groups of antimicrobial peptides (AMPs)[1] are found, defensins and cathelicidin-derived peptides. Both have two distinct roles, antimicrobial activity and serving as signaling molecules on the borderline of innate and acquired immunity (*2*, *3*).

Defensins are short cationic peptides 28−42 amino acids in length usually containing three intramolecular disulfide bonds (*4*−*6*). Their mode of action involves electrostatic interactions with the membrane, leading to permeability changes or pore formation in bacteria, fungi membrane, and viruses' envelopes (*1*, *7*). The low degree of sequence similarity among members of the mammalian β-defensin family, in addition to the highly conserved secondary and tertiary structures as well as similarities of charge density, suggests that their antimicrobial activity may depend on the structure and charge distribution rather than their primary sequence (*8*). Because they lack a distinct hydrophobic core, folding of defensins is mainly stabilized by the presence of three disulfide bonds (*9*). Studies of peptide analogues of human β-defensin-3 (hBD-3) (*2*, *10*, *11*) have pointed to the distribution of the positively charged amino acids and hydrophobic side chains as important parameters of antimicrobial activity, while the overall hydrophobicity may correlate with cytotoxicity to mammalian cells.

Our previous work demonstrated that selected linear analogues of hBD-3 (full length, G1−K45) might exhibit significantly higher antimicrobial activity with lower cytotoxicity than the

[†]This work was supported by the Nanyang Technological University URECA program and National Medical Research Council of Singapore (NMRC) Grants 1106/2007, 0808/2003, CPG/007/2004, and NMRC-IBG. This work was also supported by academic research fund (AcRF) Tier 2 by the MOE (Grant T206B3210RS).

*To whom correspondence should be addressed. R.W.B.: Singapore Eye Research Institute, 11 Third Hospital Avenue, #06-00, Singapore 168751; fax, (+65) 6322-4599; e-mail, rbeuer@pacific.net.sg. Y.M.: School of Biological Sciences, Nanyang Technological University, Nanyang Drive 60, Singapore 637551; e-mail, ygmu@ntu.edu.sg. K. P.: School of Biological Sciences, Nanyang Technological University, Nanyang Drive 60, Singapore 637551; fax, (+65) 6791-3856; e-mail, kpervushin@ntu.edu.sg; telephone, (65)-65141916.

[1]Abbreviations: Acm, acetamidomethyl; AMP, antimicrobial peptide; cfu, colony forming unit; COSY, correlation spectroscopy; DMPC, 1,2-dimyristoyl-*sn*-glycero-3-phosphocholine; DHPC, 1,2-diheptanoyl-*sn*-glycero-3-phosphocholine; DPC, dodecylphosphocholine; DOSY, diffusion-ordered spectroscopy; ESI-MS, electrospray ionization mass spectrometry; hBD, human β-defensin; hBD-3, human β-defensin-3; HPLC, high-performance liquid chromatography; HSQC, heteronuclear single-quantum coherence; LPS, lipopolysaccharides; NMR, nuclear magnetic resonance; NOE, nuclear Overhauser effect; NOESY, nuclear Overhauser effect spectroscopy; POPG, 1-palmitoyl-2-oleoyl-*sn*-glycero-3-[phospho-*rac*-(1-glycerol)]; SERI, Singapore Eye Research Institute; SGH, Singapore General Hospital; rmsd, root-mean-square deviation; ROE, rotational frame Overhauser effect; ROESY, rotational frame Overhauser effect spectroscopy; TOCSY, total correlation spectroscopy; w/v, weight/volume.

Published on Web 07/06/2009

Table 1: Biophysical Properties of Three hBD-3 Analogous Peptides

peptide	molecular weight	pI (iso-electric point)	overall hydrophobicity[a]	net (+) charge	no. of hydrophobic residues	sequence[b]
C2	1432.79	11.57	19	7	0	RGRK**CC**[c]RRKK
F2	1378.7	12.9	16	7	2	RGRK**FF**RRKK
Y2	1410.69	11.59	16.4	7	2	RGRK**YY**RRKK

[a] Hydrophobicity is calculated on the basis of the Hopp−Wodds hydrophilicity scale. A lower value corresponds to a lower hydrophilicity. [b] Residues modified from original native peptide sequence are highlighted in bold. [c] Cysteine residues are acetamidomethyled, C(Acm).

native protein (*12*). The latter effect is related to the removal of disulfide bridges resulting in increased structural flexibility of the linear forms. Since peptides with varying hydrophobicity values are found to be potent antimicrobials, there are apparently unknown determinants of the three-dimensional (3D) structure that balance charge density and hydrophobicity. Although defensins as with any other antimicrobial peptide must first penetrate an outer barrier, e.g., mainly lipopolysaccharides (LPS) and peptidoglycan in bacteria or a glycocalix layer and matrix proteins in mammalian cells (*13*−*15*), the main target is the lipidic plasma membrane (*12*, *13*, *16*). A simulation of the lipid composition of bacterial membranes can be used as a target to predict antimicrobial potency (*17*). Thus, understanding bacteria killing mechanisms by antimicrobial peptides requires studies at atomic resolution of the intrinsic structural properties of peptides as well as their modulation by model membranes.

As we demonstrate in this study, some of the newly designed, even shorter defensin C-terminal analogues (R36−K45) exhibit improved antimicrobial activities with minimal cytotoxicity. Three C-terminal (R36−K45) analogues of hBD-3, C2, Y2, and F2, were selected so their 3D structures and interaction with membrane lipids could be studied using NMR spectroscopy and MD simulations (Table 1). We found that the ability of these peptides to dimerize both in aqueous solution and on the membrane surfaces leads to a large increase in the local positive charge density (*18*). This seems to be an important feature for these peptides to increase both the affinity and possible interface area interacting with lipid membranes. Moreover, as indicated by MD simulations, accretion of a well-defined structure featuring the most compact density of positive charges leads to a more efficient bactericidal activity. Our studies suggest that the higher density of positive charges within the scaffold of well-defined structure might predict higher antimicrobial activity.

MATERIALS AND METHODS

Peptide Selection and Synthesis. A series of human β-defensin-3 (hBD-3) C-terminal (R36−K45) analogues were produced using solid phase peptide synthesis (SPPS), via either chemical modification of two cysteine residues in the original sequence or substitution of them with other amino acids. The series of hBD-3 C-termianl (R36−K45) analogues was derived and named by the two amino acids in the center of the sequences, at the two Cys positions. HPLC and ESI-MS were subsequently performed for peptide purification and identification. Following antibacterial and cytotoxicity assays, C2, F2, and Y2 peptides were selected for structural analyses. The original hBD-3 C-terminal (R36−K45) sequence is RGRKCCRRKK. The C2 sequence is RGRKC(Acm)C(Acm)RRKK (Acm, acetamidomethyl group). The F2 sequence is RGRKFFRRKK. The Y2 sequence is RGRKYYRRKK.

Antimicrobial Activity Assays. The bacterium *Pseudomonas aeruginosa* ATCC 9027 was used in this study. It was chosen because *P. aeruginosa* is known to cause corneal ulcers that are difficult to treat and require an intensive regimen of fortified topical antibiotics. Resistance to some commonly used antibiotics has been documented among clinical ocular isolates of *P. aeruginosa*, thus adding to a sense of urgency in the search for alternative therapeutic agents (*19*). Bacteria were no more than five passages removed from the original master lot obtained from the American type Culture Collection (ATCC). Bacteria were prepared with a final cell count of 10^5−10^6 cfu/mL. The cfu of surviving bacteria were counted after incubation with test peptides at 22.5 °C for 4 h in purified water media. The antibacterial activity of the peptide was manifested as the logarithmic reduction of the bacteria on exposure to the peptide. Peptides that exhibited high bacterial killing activities were subsequently selected and tested in high-salt restricted conditions [0.9% (w/v) sodium chloride buffer and incubation for 6 h]. Bacteria unexposed to peptides were also counted parallel to the test as a control.

Cytotoxicity Assay. For the cytotoxicity assays, the primary concern was for the fragile epithelial cells that cover the surface of the eye. This is a mucosal surface, and an important use of AMPs would be for the eye or other mucosal surfaces such as the lungs and mouth, all of which have an epithelial cell covering (*12*). Cytotoxicity was determined by measuring the amount of ATP generated by viable cells in culture using the CellTiter-Glo luminescent cell viability assay (Promega, Madison, WI). Synthesized peptides were incubated with a human conjunctival epithelial cell line (IOBA-NHC) as described previously (*12*, *20*). The luminescent signal was read by a microplate reader (Tecan GeniosPro, Tecan Asia, Singapore). Blank wells containing only medium were included in each assay, and the reading was subtracted from each sample and control well. Using the luminescence of the untreated wells as 100%, the cell viability was calculated as (luminescence of the control − luminescence of the sample)/luminescence of the control × 100%. Each condition was assayed in triplicate, and the experiments were repeated three times.

Hemolysis Assay. The hemolytic activity of the peptides was estimated by the amount of hemoglobin released from rabbit erythrocytes (*12*). Rabbit erythrocytes were chosen because AMP-induced toxicity easily occurs in these blood cells when compared to human red blood cells (*21*). The hemolytic activity of each sample was calculated as $(OD_{sample} - OD_{blank})/(OD_{positive\ control} - OD_{blank}) \times 100\%$. Each condition was assayed in triplicate, and the experiments were repeated three times. Rabbit procedures were approved by the IACUC of SingHealth.

NMR Sample Preparation. DPC (5.27 mg) (Avanti Polar Lipids) with or without 1.16 mg of POPG (Avanti Polar Lipids) was directly dissolved in 0.5 mL of 30 mM phosphate buffer. This resulted in 30 mM DPC or 10:1 (molar ratio) DPC−POPG membrane mimicking solutions. DMPC (41 mg) (Avanti Polar Lipids) was

dissolved in ethanol and dried under a N_2 stream. DHPC (11 mg) (Avanti Polar Lipids) was dissolved in 30 mM phosphate buffer and used to solubilize DMPC. After several cycles of freezing and thawing, the mixture was a 10% (w/v) DMPC/DHPC bicelle solution with a "q" factor of 3 (DMPC:DHPC molar ratio of 3:1). Relatively large bicelles ($q = 3$) were made to provide a large planar region in its discoidal structure and, hence, a better mimic to a membrane bilayer (*22*, *23*). The peptide stock solutions were directly added to the lipid-containing solutions.

NMR Experiments. NMR experiments were performed using Bruker Avance II 600 and 700 MHz spectrometers at 25 °C for aqueous and micelle solutions and 10 °C for the discord bicelle medium. In the latter case, the lower temperature was used to maintain the isotropic tumbling of bicelles (*23*).

Two-dimensional (2D) homonuclear TOCSY, NOESY, and ROESY experiments were conducted with mixing times of 70, 150, and 100 ms, respectively, using 500 μM peptides at pH 5. The Y2 peptide was analyzed in the complex with DPC−POPG mixed micelles and DMPC/DHPC bicelles. F2 and C2 peptides were analyzed in complex with DPC−POPG mixed micelles. Data were collected for each experiment for 7 h. Residue specific resonance assignment and assignment of NOESY cross-peaks were performed using CARA (www.nmr.ch). 3D structures of Y2 and F2 peptides in DPC−POPG mixed micelles and Y2 in DMPC/DHPC bicelles were reconstructed using CYANA 2.0 (*24*).

2D $^1H-^{13}C$ HSQC experiments using natural abundance ^{13}C in 5 mM peptide samples were also performed. HSQC spectra of both F2 and Y2 peptides dissolved in a DPC−POPG mixed micelle solution were recorded. A bicelle solution was not used in this experiment since Y2 showed no secondary structure differences in micelle or bicelle solutions. Urea (8 M) was added to each sample subsequently for collection of reference spectra of denatured peptides.

A series of one-dimensional (1D) ^1H homonuclear experiments were conducted for each sample with increasing peptide concentrations (10, 20, 50, and 500 μM), both in phosphate buffer and in 30 mM DPC solutions.

DOSY experiments were performed for each peptide sample in phosphate buffer, 30 mM DPC micelles, and DPC−POPG (30 mM DPC and 3 mM POPG) mixed micelles (*25*). The pulsed magnetic field gradient strength was calibrated using the ^1H signal in a 99.9% D_2O sample with the self-diffusion coefficient of HDO [$(1.902 \pm 0.002) \times 10^{-9}$ m^2/s]. A series of 1D spectra were measured with a diffusion delay of 150 ms and increasing gradient strength in 32 steps from 2 to 95% of G_{max}. Diffusion coefficient D_S is calculated by fitting the curve of signal intensity versus variable gradient strength. The molar fraction of peptide in lipid (F_L) is calculated with eq 1 (*25*)

$$D_S = D_L F_L + D_F(1 - F_L) \quad (1)$$

where D_L and D_F are the diffusion coefficients of lipid micelles and free peptides in DPC solution, respectively.

Molecular Dynamics Simulations. Six sets of Hamiltonian replica exchange molecular dynamics (hREMD) simulations were conducted for C2, F2, and Y2 peptides with eight replicas each at a temperature of 300 K. The details of this hREMD method can be found in recent work (*26*). The novel part of the method is that instead of reducing the intermolecular interactions, we increased the repulsive part of the van der Waals interactions between the peptide atoms. The dissociation-enhanced hREMD method decreases the energy barrier between local minima which are mainly stabilized by non-native contacts. Thus, such hREMD simulations helped to sample a broader range of configurations of peptide oligomers. For each peptide dimer, two hREMD simulations were performed with different initial configurations: one begun with the NMR-derived dimer structure and the other started with the two monomers separated. For C2 and F2 peptides, simulations provided converged results by 100 ns, while for Y2 peptides, 150 ns simulations were needed. Twenty of each Y2−F2 dimer conformer reconstructed from NMR data were clustered on the basis of the pairwise rmsd with a cutoff of 1 Å. The center of the largest cluster was selected as a representative conformer of the dimer. The two tyrosine residues of the Y2 model were changed to two cysteine residues to build a model of the C2 dimer. The C2, F2, and Y2 models were separately solvated with explicit water in simulation boxes. The complex is formed when the minimum distance between the two monomers is less than 0.375 nm. The complex structures from the Y2 and C2 dimer simulations were analyzed to extract binding free energies using the MM/GBSA protocol (*27*).

Table 2: Assays of Antimicrobial Activity of Defensin's Derived Peptides against *P. aeruginosa* ATCC 9027 (log reduction)[a]

	low salt (4 h)				high salt (6 h)	
concn (μg/mL)	C2	F2	H2	Y2	Y2	W2
200	0.41	0.33	0.29			
100	0.57	0.61	0.62		4.19	
50	0.63	0.87		3.07	4.07	1.06
25				2.39	3.31	0.48
12.5				2.10	0.49	0.09
6.25				2.02	0.49	0.08
3.125				0.33		

[a] Peptides were incubated with *P. aeruginosa* ATCC 9027 for 4 h at 22.5 °C. A 0.5 log reduction equals 68% of the bacteria being killed, a 1 log reduction 90% of the bacteria, a 2 log reduction 99% of the bacteria, and a 3 log reduction 99.9% of the bacteria.

The micelle structure was modeled using 64 DPC molecules (M64) (*28*). A single DPC molecule was extracted from a 65-mer DPC micelle provided by the Tieleman group (*29*). The molecule was repeatedly copied, rotated, and translated to generate a 64-mer DPC micelle. The complete parameter set for bonded, nonbonded, and 1−4 interactions of the lipid atoms as well as the nonbonded interactions between lipid and peptide atoms was provided by the Tieleman group and combined with the OPLS-AA force field in the Gromacs package.

Two different initial setups with regard to the relative position of the Y2 dimer with the micelle were constructed. In one case, the Y2 dimer was placed in the middle of M64, while in the other case, the peptide was placed in the solvated water in the proximity of the external surface of M64. In these two simulations, distance restraints with a force constant of 3000 kJ mol^{-1} nm^{-2} were imposed on the peptide to maintain the backbone structure of the NMR model while allowing free motion of the side chains. The restraints were imposed across intramonomer backbone heavy atom pairs (Cα, N, and C′) and across intermonomer Cα atom pairs. The peptide−micelle complex was solvated in a cubic box with dimensions of 7 nm × 7 nm × 7 nm with 9720 explicit TIP3P water molecules and 14 chloride ions, thus neutralizing the net charge on the system.

The MD simulations were implemented using the Gromacs package applying the OPLS-AA (all-atom) force field (*30*). The

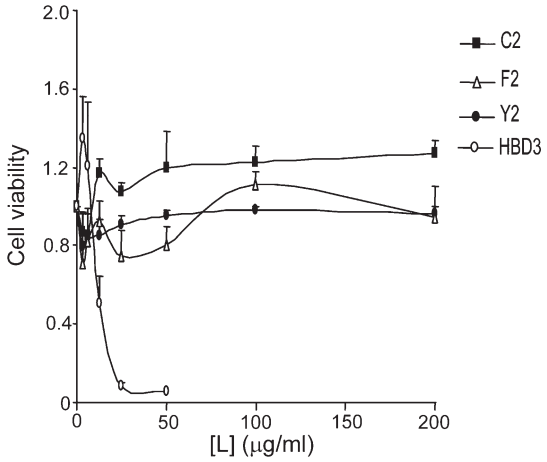

FIGURE 1: Cytotoxicity assay of C2 (■), F2 (△), and Y2 (●) peptides for human conjunctival epithelial cells. Data for human β-defensin-3 (hBD-3) are also given (○). Reported values are means of performed experiments with variation bars representing the standard deviation (rmsd).

Table 3: Peptide Lipophilicity Measurement (F_L)

	F_L[a] (%)		
	C2	F2	Y2
DPC	35.17	31.25	41.41
DPC−POPG	100	100	100

[a] F_L is the molar fraction of peptides bound to the lipid phase.

Table 4: Translational Diffusion Coefficients of C2, F2, and Y2 Measured by NMR

	D_S[a] ($\times 10^{-10}$ m^2/s)		
	C2	F2	Y2
5 μM	5.32 ± 0.17	5.5 ± 0.23	5.71 ± 0.19
500 μM	2.37 ± 0.10	2.31 ± 0.23	2.01 ± 0.03

[a] D_S is the translational diffusion coefficient.

complete parameter set for bonded, nonbonded, and 1−4 interactions of the lipid atoms was the Berger force field; the protein interactions were described by the OPLS-AA force field. To treat the difference of the 1−4 interaction scale factor in Berger (1.0) and OPLS-AA (0.5), the half-ε double-pair list method was applied. All bonds connected to hydrogen atoms were constrained in length according to the LINCS protocol. The protein, DPC, water, and ions were separately coupled to an external heat bath with a relaxation time of 0.1 ps. Electrostatic interactions were treated with the particle mesh Ewald method with a cutoff of 9 Å, and a cutoff of 14 Å was used in the calculation of van der Waals interactions. The simulated systems were energy-minimized using a steepest descent algorithm for 2000 steps and then simulated for 100 ps with the position of all heavy atoms restrained to allow water molecules to relax prior to a simulation run. The generalized Born (GB) calculations were performed using the sander module in AMBER 9. The source code of Amber was modified to allow the use of the OPLS-AA force field. The modified GB model developed by A. Onufriev, D. Bashford, and D. A. Case was used (*31*).

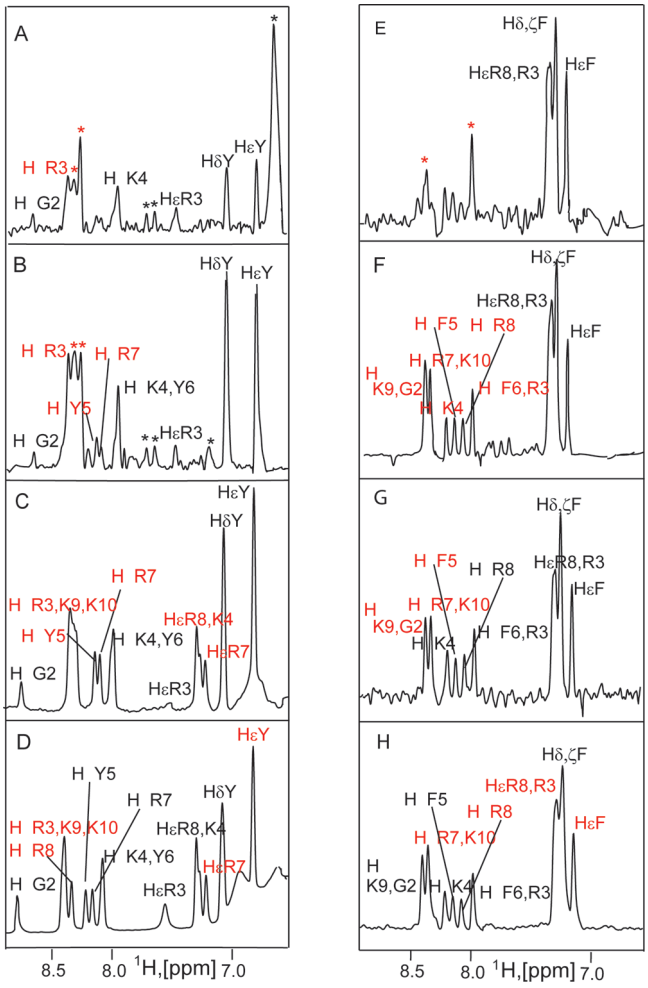

FIGURE 2: 1D ^{1}H spectra of Y2 (A−D) and F2 (E−H) as a function of concentration in the presence of 30 mM DPC at 25 °C. The concentrations of the peptides are (A and E) 10 μM, (B and F) 20 μM, (C and G) 50 μM, and (D and H) 500 μM. ^{1}H peaks are assigned and labeled. Unknown peaks which could not be assigned are labeled with stars. Gradually changing proton resonance peaks are highlighted in red. Spectra in each column share the common axis labeled at the bottom (D and H).

RESULTS

Antibacterial Activity Assays. Defensin-derived peptides exhibited varying antibacterial activities against the common human pathogen *P. aeruginosa* ATCC 9027. The results are listed in Table 2. The Y2 peptide exhibited high antibacterial activity in the low micromolar range under both conditions compared to the other peptides. A cooperative increase in the activity of Y2 was detected at concentrations from 3.2 to 6.3 μg/mL (2.5−5.0 μM) under aqueous conditions and from 12.5 to 25 μg/mL (10−20 μM) under salt conditions. This suggests a structural transition of Y2 in the 5−20 μM concentration range, resulting in its remarkably increased activity. In contrast, relatively low antibacterial activity was observed for concentrations of C2 and F2. Up to 100 μM, no detectable transitions to a high-activity state were observed in either peptide in aqueous solution. Y2 was selected as a representative of the high-activity group for subsequent structural studies, while in the low-activity group, C2 was selected to represent a native peptide and the F2 peptide was selected because of its high degree of sequence similarity to the Y2 peptide.

Cytotoxicity and Hemolytic Activity against Mammalian Cells. The cytotoxicity of hBD-3 analogues was tested on a

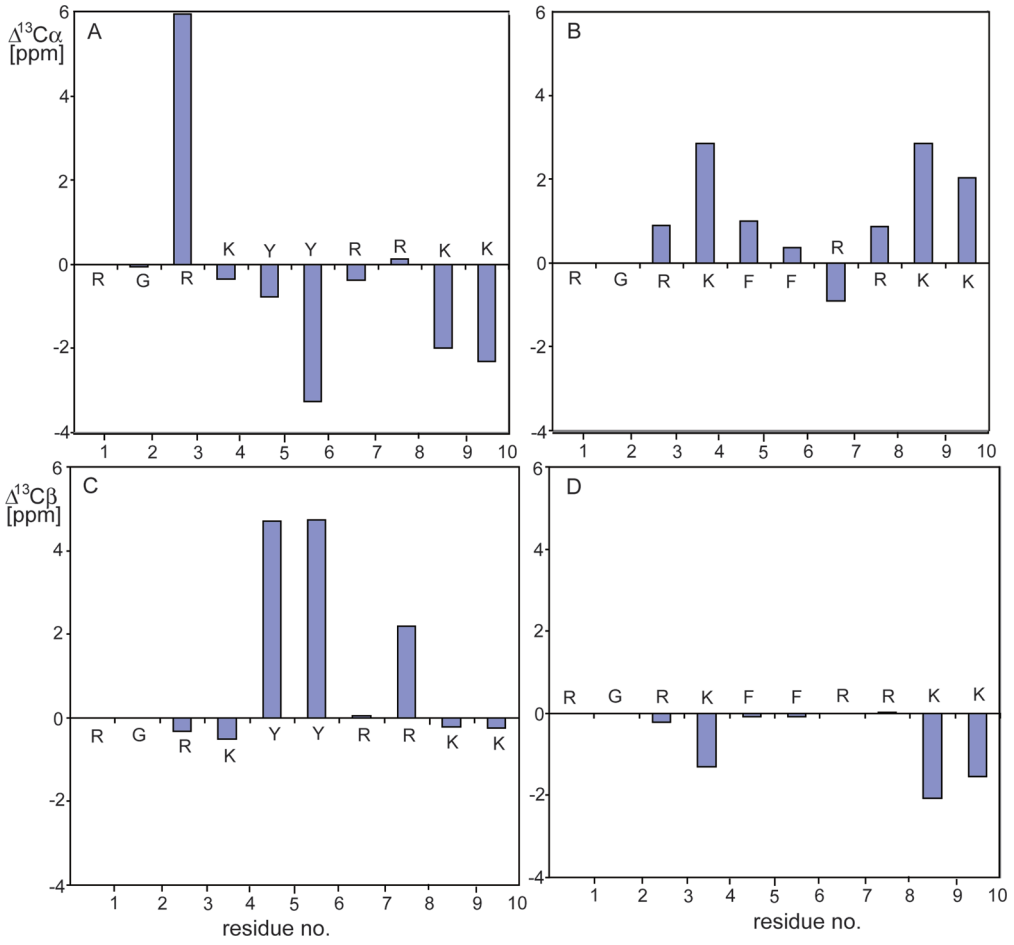

FIGURE 3: Peptide secondary chemical shift plot (Cα and Cβ region). Both Y2 and F2 peptides' secondary structures in lipids environment (30 mM DPC and 3 mM POPG in 30 mM phosphate buffer) were compared to those in urea added as a reference. Panels A and C are plots for Y2 peptides, while panels B and D are plots for F2 peptides.

human conjunctival epithelial cell line (IOBA-NHC cells). No decrease in viable cell number was observed 24 h after constant exposure to C2, F2, or Y2 at concentrations up to 200 μg/mL (Figure 1). A slight increase in the viable cell number was observed in the presence of C2 in the concentration range of 12.5−200 μg/mL. On the other hand, native hBD-3 at 12.5 μg/mL resulted in ~50% epithelial cell death, corroborating an earlier observation (*12*). Only 6% of the cells remained viable after exposure to hBD-3 for 24 h at 50 μg/mL. Hemolytic activities of both peptides were also measured using freshly isolated rabbit erythrocytes. At a concentration of 200 μg/mL, < 4% of the cells were lysed by C2, F2, and Y2; hBD-3 exhibited significantly higher hemolytic activity under the same conditions.

Lipid Phase Partition of the Peptides. To characterize the affinity of C2, F2, and Y2 peptides for the lipid phase, translational diffusion coefficients (D_S) of free peptides and peptide−micelle complexes were measured using DOSY experiments (*32*). Pure DPC and mixed DPC−POPG micelles were used to represent mammalian and bacterial cell membranes, respectively. Table 3 shows the molar fractions of peptides bound to micelles (F_L) calculated using the measured diffusion coefficients (*25*). This parameter reflects the lipophilicity and affinity of the peptides for the lipid membranes. Partitioning in zwitterionic DPC micelles was only ~40% for all peptides, in contrast to the full localization into the same lipid phase doped with anionic POPG lipids. This observation was consistent with their high antimicrobial activity and low cytotoxicity.

Structural Transitions in C2, F2, and Y2. The diffusion coefficients of C2, F2, and Y2 peptides at high (500 μM) and low (5 μM) concentrations in phosphate buffer were also measured in DOSY experiments. Results are listed in Table 4. It is interesting to note that for all three peptides, the diffusion rate at 5 μM was approximately double that at 500 μM. According to the Stokes−Einstein equation, the peptide diffusion rate is in reverse proportion to molecular size. This means at concentrations above 500 μM in aqueous solution all three peptides form stable dimers while at concentrations below 10 μM monomeric forms predominate.

To monitor the monomer−dimer transition concentration and peptide structure changes, 1D (^{1}H) spectra of C2, F2, and Y2 in the presence and absence of DPC micelles were recorded at peptide concentrations of 10−500 μM. These spectra were used to monitor peptides' structural transitions, which can be reflected by changes in the ^{1}H resonance positions. In the absence and presence of DPC micelles, both peptides underwent structural changes likely induced by dimerization. Figure 2 shows 1D proton spectra of Y2 and F2 as a function of concentration dissolved in a 30 mM DPC micelle solution. Gradually changing proton resonance peaks are highlighted in red. In the ^{1}H spectra at a peptide concentration at 20 μM (Figure 2B,F), resonances stemming from monomeric (Figure 2A,E) and dimeric (Figure 2C,G) forms could be detected, indicating the slow (on the time scale of ^{1}H chemical shifts) kinetic regime of exchange between these two forms. Although C2 exhibits similar structural

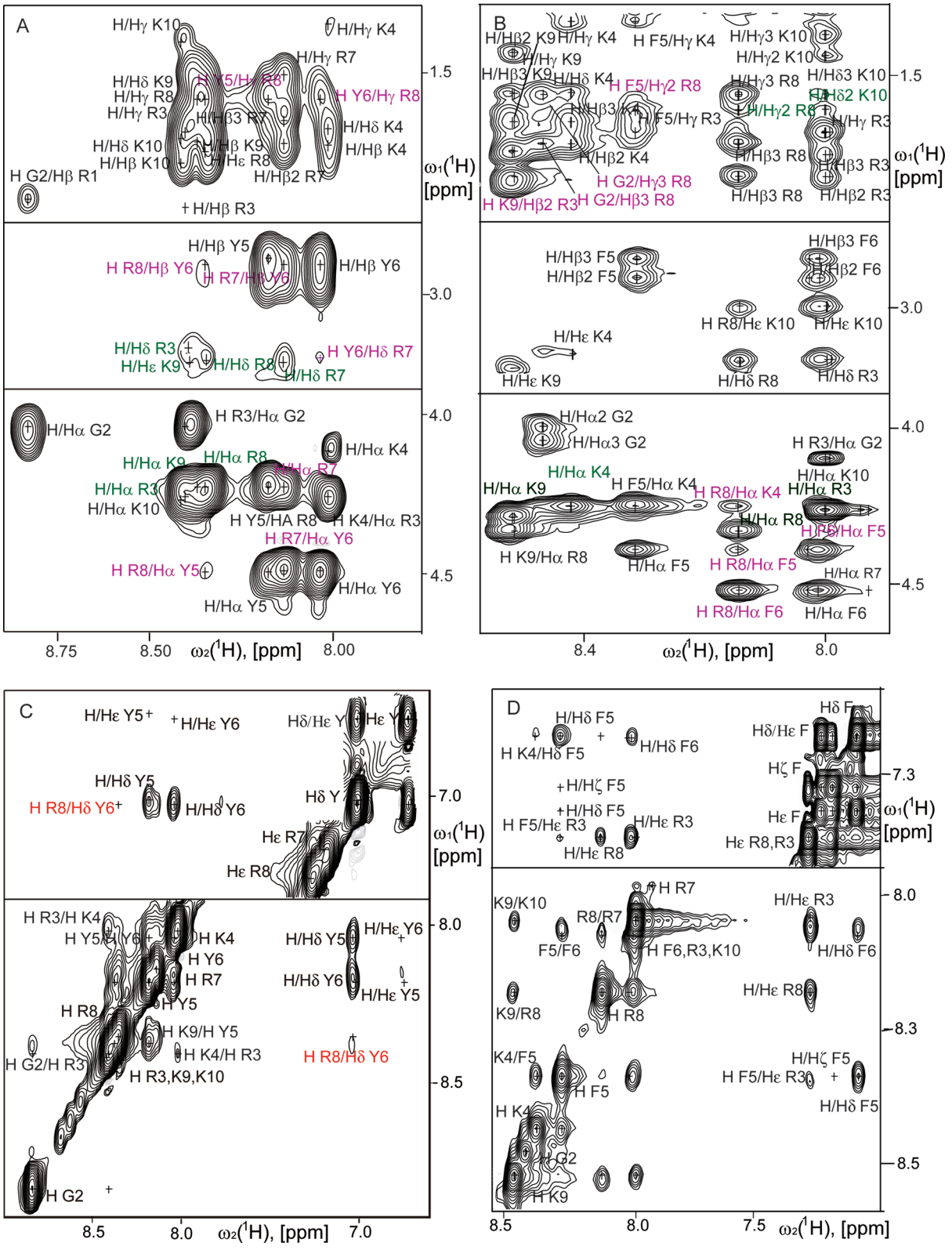

FIGURE 4: 2D NOESY spectra of Y2 (A and C) and F2 (B and D). Y2 or F2 peptide (500 μM) was dissolved together with 30 mM DPC and 3 mM POPG in 30 mM phosphate buffer (pH 5). Amide−aliphatic proton regions are shown in panels A and B, and diagonal portion regions are shown in panels C and D. The proton specific assignment of individual NOESY cross-peaks is indicated. In panels A and B, intermolecular NOEs between peptide monomers and peptide and detergent are highlighted in pink and green, respectively. In panel C, a particular NOE which may indicate the formation of a hydrogen bond between the Tyr6 side chain on one monomer and the Arg8 backbone on the other monomer of the dimeric structure is highlighted in red.

changes, Y2 and F2 formed dimers at a significantly lower transition midpoint of ~20 μM while C2 dimerized around 500 μM. Minor structural changes with further peptide concentration increases could also be observed. 1D spectra of Y2 and F2 in water showed structural monomer−dimer transitions as well over the concentration range of 50−100 μM. This indicated that DPC micelles could promote peptide dimerization at lower concentrations than in aqueous solution, presumably stabilizing

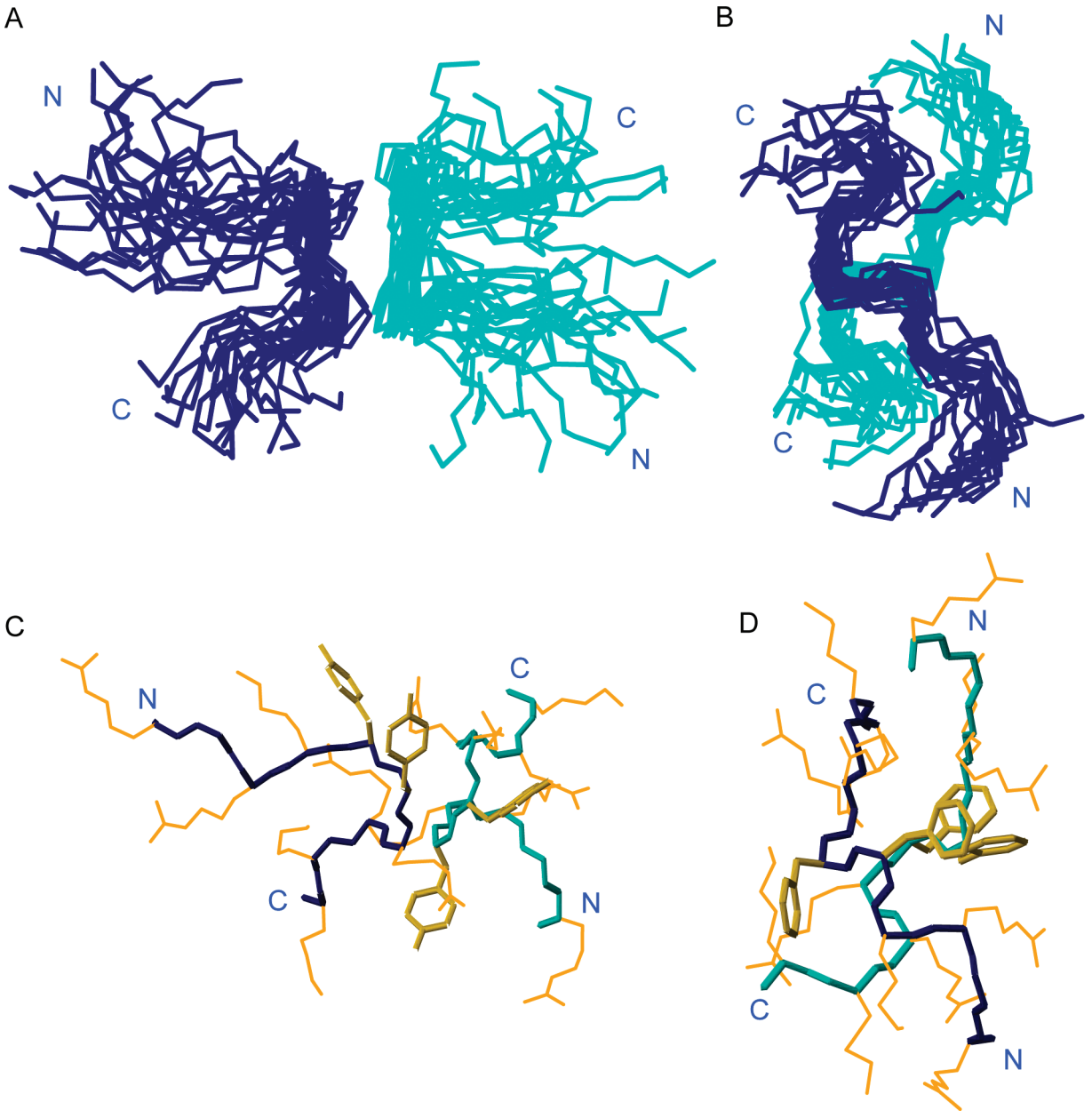

FIGURE 5: NMR structures of dimeric Y2 and F2 peptides in the presence of DPC−POPG mixed micelles (30 mM DPC and 3 mM POPG). Panels A and B are superpositions of 20 Y2 and F2 conformers, respectively; panels C and D are representative conformers of Y2 and F2 peptides, respectively. Aromatic side chains are highlighted in gold, and heavy atom side chains of charged amino acid residues are colored orange. The backbone of individual monomers in the dimeric structure is colored royal blue and dark green. The N- and C-termini of each monomer are indicated. Figures were prepared using Molmol (*57*).

the peptide dimer at the surface of the lipid membrane. A similar effect was also observed for the C2 peptide. The monomer−dimer transition of Y2 correlated with its cooperatively increased activity in the same concentration range. In contrast, the C2 peptide, which exhibits only low antibacterial activity at all the concentrations that were studied, underwent the dimerization transition at much higher concentrations. In addition, F2 dimerizing at low concentrations but lacking high bactericidal activity suggests that features other than the dimerization ability are also important determinants for the activity of these peptides.

3D NMR Structures of F2 and Y2. 2D NOESY spectra of Y2 and F2 in DPC−POPG mixed micelles (Figure 3) were used to reconstruct detailed 3D structures. In Figure 3, intermolecular NOEs of peptide−peptide and peptide−lipid interactions are highlighted in red and green, respectively. The mobility at side chains in F2 appears to be more restricted than in Y2 because of systematic removal of chemical shift degeneracy of two protons in methylene groups of F2 but not in Y2. Striking differences in NOE patterns between these peptides are seen in the amide region, indicating the presence of helical structure in F2 in contrast to predominantly turn or β-sheet structure in Y2. Initially, 63 (Y2) and 72 (F2) intramonomeric NOEs were identified and used for structural reconstruction of the monomers. Subsequently, 14 (Y2) and 20 (F2) NOEs which could not be satisfied with the monomeric structure were assigned as intermonomeric and used for dimeric structure calculations. Remarkably, C2 in DPC−POPG mixed micelles exhibited overall a significantly smaller number of NOEs with markedly reduced intensities in comparison to the diagonal peaks. This prompted us to measure 2D ROESY spectra of the C2 peptide to

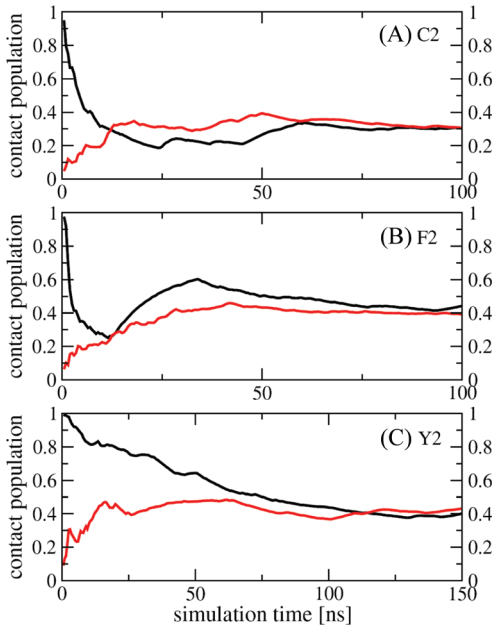

FIGURE 6: Probability of dimer formation as a function of simulation time for (A) C2, (B) F2, and (C) Y2. The simulations began with different initial configurations: dimer structure (black curves) and two separated monomers (red curves).

extract structural information. The 2D ROESY spectrum of C2 exhibited fewer structurally significant NOEs, precluding unequivocal reconstruction of the detailed 3D structure of the C2 dimer.

To investigate the effect of the lipid phase surface curvature on the oligomerization and structure of the peptides, we prepared relatively large bicelles ($q = 3$) to maximize the planar surface area of the lipid bilayer accessible to the peptides. Correspondingly, the lower temperature was used to maintain isotropic tumbling of the bicellar phase, since the temperature above 42 °C increases the degree of alignment of bicelles resulting in a lamellar phase sample which is less suitable for high-resolution NMR study. The NMR structure of Y2 in bicelles exhibited only minor differences from the Y2 structure in micelles, thus ruling out the effect of accessible surface curvature on the oligomerization and structure of Y2. The NOESY spectrum of Y2 in bicelles and the ROESY spectrum of C2 in DPC−POPG mixed micelles can be found in the Supporting Information.

The difference in the secondary structure in Y2 and F2 peptides is directly evident in the patterns of the ΔCα and Δ$C\beta$ secondary chemical shifts of two peptides relative to their respective random coil shifts induced by 8 M urea (Figure 4). Both ΔCα and Δ$C\beta$ patterns in F2 and Y2 peptides are generally opposite to each other, indicating the prevalence of helical structure in F2 and turn or β-sheet structure in Y2.

Panels A and B of Figure 5 show 20 representative Y2 and F2 dimer conformers, respectively, superimposed using backbone atoms of residues 3−7 of both monomers. A selected conformer of each peptide is shown in panels C and D of Figure 5, respectively. The dimeric structures of both peptides arise from an antiparallel assembly of two monomeric peptide chains. Y2 comprises two turns at residues 3 and 6 connected with the otherwise extended strand of amino acids. Charged residues at the N- and C-termini of monomers are structurally disordered, while the hydrophobic center (tyrosine residues) is constrained and serves as the dimer interface. In contrast to the hairpinlike structure in Y2, the F2 dimer is formed by two helixlike

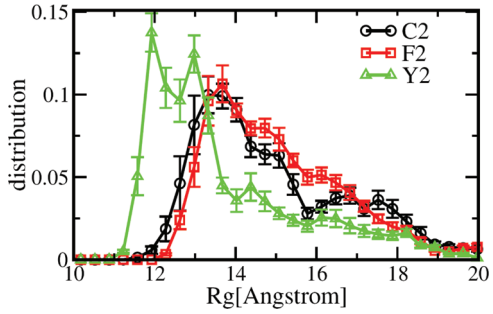

FIGURE 7: Distribution functions of the radius of gyration for charged points in C2, F2, and Y2 dimers.

Table 5: Breakdown of the Average Binding Energy between Monomers in Y2 and C2 Dimeric Configurations Estimated from MD Simulation Trajectories

energy component[a]	Y2 dimer	C2 dimer	difference
ΔE_{vdw} (kJ/mol)	−156 ± 13	−84 ± 14	−72
ΔE_{elec} (kJ/mol)	337 ± 77	537 ± 151	−200
ΔE_{gb} (kJ/mol)	−3386 ± 174	−3583 ± 289	198
ΔE_{surf} (kJ/mol)	−12 ± 1	−7 ± 1	−5
ΔE_{p} (kJ/mol)	−3048	−3046	−2
ΔE_{np} (kJ/mol)	−168	−91	−77
ΔE_{total} (kJ/mol)	−3216	−3137	−79

[a] E_{vdw} and E_{elec} are the van der Waals and electrostatic interaction energies, respectively, calculated by the Gromacs package for the peptides only. E_{gb} and E_{surf} are solvation energies of polar and nonpolar residues, calculated by Amber 9 using the Generalized Born model. E_p and E_{np} are the sums of polar energy ($E_{elec} + E_{gb}$) and nonpolar energy components ($E_{vdw} + E_{surf}$), respectively. E_{total} is the sum of E_p and E_{np}.

monomers twisted around each other. The central region formed by aromatic side chains (Phe) contributes to stabilization of the intermonomeric interface.

Molecular Dynamics Simulations. To further examine the structure−activity relationship of the peptides, six sets of Hamiltonian replica exchange molecular dynamics simulations were conducted. The probabilities of dimer formation are found to be converged within 100−150 ns simulations. This was further confirmed by repeating these simulations with different initial configurations of each peptide. F2 and Y2 have a similar dimer formation probability of 40% which is somewhat larger than that of C2 (30%) (Figure 6).

Since the local charge distribution and density within the peptides were suggested to be important factors of their antibacterial actions (*8*), we analyzed the simulations for these properties. The positions of atoms Nζ and Cζ on the side chains of Lys and Arg residues were taken as the representative charge positions, which resulted in 14 "charged" points in each peptide dimer. The radius of gyration of these charged points (^cR_g) reflects the distribution of charges within the peptides (Figure 7). The distributions of ^cR_g of C2 and F2 dimers are similar; both are peaking around an R_g of 13.5 Å with long slow-decaying tails. Counterintuitively, the distribution of ^cR_g for the Y2 dimer is very different. The largest peak is located at a ^cR_g of 12 Å, and the distribution drops sharply when $^cR_g > 13$ Å. The charge density is estimated using eq 2:

$$\rho = Q/V = \frac{Q}{4/3\pi c\overline{R_g^3}}, \qquad (2)$$

where Q is the total charge of a peptide dimer (Q = 14e for all peptides). The average ^cR_g for C2 and F2 dimers is 14.9 ± 0.25 Å

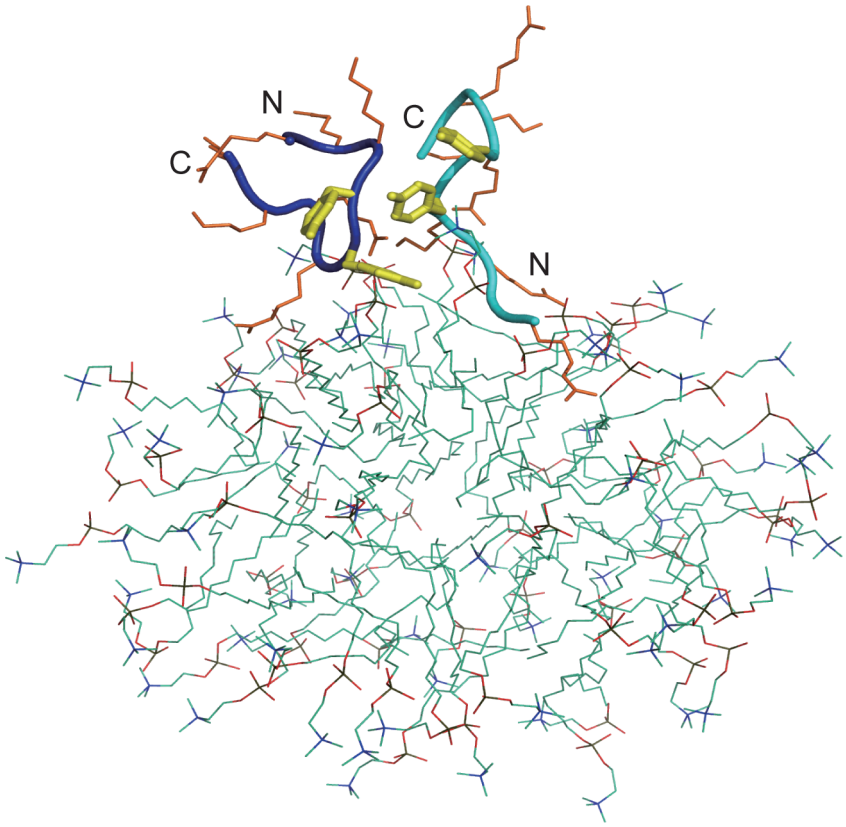

FIGURE 8: Representative snapshot of the Y2−DPC configuration in the 30 ns long MD simulation run. The Y2 dimer is highlighted as tubes. DPC molecular bonds containing oxygen, nitrogen, and carbon are colored red, blue, and green, respectively. This figure was prepared with PyMol (DeLano Scientific LLC).

each, and the average $^{c}R_g$ of the Y2 dimer is 13.6 ± 0.28 Å. The charge density of the C2 and F2 dimer is $(1.0 \pm 0.05) \times 10^{-3}$ e/Å^3, while the charge density of the Y2 dimer is $(1.3 \pm 0.07) \times 10^{-3}$ e/Å^3. The charge density of Y2 is 30% higher than that of C2 or F2. For the sake of comparison, the charge density of the C-terminus of hBD-3 (R36−K45) [Protein Data Bank entry 1KJ6 (*33*)] was calculated in a similar way: from residue 32 to 45, the total charge is 8e with a $^{c}R_g$ of 12.3 Å, resulting in a ρ of 1.03×10^{-3} e/Å^3, which is comparable to that of C2 and F2.

Table 5 shows the average binding free energies estimated from the final 2 ns simulations of the solvated Y2 and C2 dimers. It is clear that the Y2 dimer is more stable and this originates in better packing, as is evident from the van der Waals energy term ($\Delta\Delta E_{vdw} \approx 72$ kJ/mol); this arises mainly from the $\pi-\pi$ stacking of the aromatic side chains of four tyrosine residues. The dimers are electrostatically unstable, with the Y2 dimer being less destabilized than the C2 dimer. However, the destabilized electrostatics is offset by solvation effects as the charged side chains are well-exposed and solvated. The net polar component of the binding energy is also more stable for the Y2 dimer but is exceedingly small [$\Delta\Delta(E_{elec} + E_{gb}) = 2$ kcal/mol], and hence, the dimerization is mainly driven by packing interactions.

Two long simulations of 50 ns were employed to study the Y2 peptide−micelle system. The simulations indicated strong interactions between the peptide and DPC headgroups driven mainly by polar contacts between charged amino acids and polar headgroups. One snapshot obtained at the simulation time of 50 ns demonstrated close contacts between the side chains of positively charged residues (Arg 1, Arg 3, Lys 4, Arg 7, and Arg 8) and the DPC phosphatidylcholine groups (Figure 8). Such interactions are expected to be even stronger for lipids with negatively charged headgroups.

DISCUSSION

Defensins are small, positively charged peptides, characterized by the presence of conserved cysteines (*6*, *8*) that are bridged by disulfide links. Although evolutionarily conserved, the native disulfide bridges are not critical for antibacterial activity, and short segments of hBD-1 to hBD-3 are potent antimicrobial agents (*2*, *34*−*43*). Disulfide bonds formed by Cys residues may not be critical for defensin antimicrobial activity but rather contribute to their overall peptide structural stability and chemotaxis activities (*2*). Similar effects can be found in other antimicrobial peptides, like tachyplesin and polyphemusins (*21*, *44*). Analogues of natural antibacterial peptides with deletion of the disulfide bonds have the advantage of removing chemotaxis and so may be nonimmunogenic as drug candidates.

In this study, we show that a human β-defensin-3 C-terminal (R36−K45) analogue peptide, Y2, with the two cysteine residues replaced with tyrosines, exhibited higher antibacterial activity against the Gram-negative bacterium *P. aeruginosa* and lower cytotoxicity against mammalian cells compared to the original full-length human defensin. The underlying physicochemical properties distinguishing Y2 and low-activity group peptides (F2 and C2) include propensities to oligomerize and to accrete unique structure both in water and on the surface of lipid membranes. Molecular dynamics simulations showed a higher stability of the Y2 and F2 dimers compared to that of C2. This originates mainly from $\pi-\pi$ stacking and hydrophobic interactions between the Tyr and Phe aromatic side chains. The oligomerization state has been studied in many antimicrobial peptides. A recent study of magainin analogue MSI-78 showed that dimerization of the MSI-78 peptide increases the electrostatic attraction for bacterial membranes and also reduces the

affinity for mammalian cell membranes whose outer leaflet is zwitterionic (*45*). The prominent structural difference between Y2 and F2 dimers might underline differences in their activity. The Y2 dimer maintains a hairpinlike, more compact configuration, in striking contrast to a twisted helical, extended structure of the F2 dimer. The compact structure of Y2 induces a higher charge density. The strong correlation of antibacterial action and surface charges has been well-studied, and our finding here is in line with the notion that the electrostatic interaction between the cationic peptides and anionic lipids is very important for the antibacterial function (*46*−*49*). In addition, the Tyr residues are involved in aromatic stacking interactions as well as in intramolecular hydrogen bonds with surrounding polar groups that in turn further stabilizes the compact configuration.

Antimicrobial peptides represent a new therapeutic candidate for overcoming antibiotic resistance issues. Understanding bacterial killing mechanisms of these peptides is necessary, so that modifications can be made to improve their pharmaceutical efficacy. Some α-helical peptides (like magainin, magainin analogue MSI-78, and pardaxin) kill bacteria via formation of bilayer-spanning pores (*48*, *50*−*54*). Very differently, β-defensins may exert their antimicrobial activity by an electrostatic charge-based mechanism (*33*, *55*). A recent study (*56*) has shown that clustering of anionic lipids onto the bacterial membrane might cause a phase boundary defect in the membrane. These defects are thought to be responsible for increased levels of membrane leakage and permeability, or altered membrane function and signaling activity (*56*). Our data point to the critical role electrostatic charge density plays in antibacterial activity, which potentially causes such a defect in the bacterial inner membrane. We are currently extending these studies to examine the interactions of these peptides with bacterial membranes using solid state NMR. However, we are finding that structural parameters such as compactness and charge density may act as filters in the design of novel antibacterial peptides or small molecule mimics.

ACKNOWLEDGMENT

We acknowledge Prof. James J. Chou (Department of Biological Chemistry and Molecular Pharmacology, Harvard Medical School, Boston, MA) for discussion about diffusion experiments and diffusion coefficient calculations. We also thank Assoc. Prof. Thorsten Wohland (Department of Chemistry, National University of Singapore) for sharing his experience about the choice of lipids for antimicrobial peptide research.

SUPPORTING INFORMATION AVAILABLE

Four figures and two tables. This material is available free of charge via the Internet at http://pubs.acs.org.

REFERENCES

1. Hancock, R. E., Falla, T., and Brown, M. (1995) Cationic bactericidal peptides. *Adv. Microb. Physiol. 37*, 135–175.
2. Dhople, V., Krukemeyer, A., and Ramamoorthy, A. (2006) The human β-defensin-3, an antibacterial peptide with multiple biological functions. *Biochim. Biophys. Acta 1758*, 1499–1512.
3. Durr, U. H., Sudheendra, U. S., and Ramamoorthy, A. (2006) LL-37, the only human member of the cathelicidin family of antimicrobial peptides. *Biochim. Biophys. Acta 1758*, 1408–1425.
4. Bevins, C. L., Martin-Porter, E., and Ganz, T. (1999) Defensins and innate host defence of the gastrointestinal tract. *Gut 45*, 911–915.
5. Diamond, G., and Bevins, C. L. (1998) β-Defensins: Endogenous antibiotics of the innate host defense response. *Clin. Immunol. Immunopathol. 88*, 221–225.
6. Ganz, T., and Lehrer, R. I. (1995) Defensins. *Pharmacol. Ther. 66*, 191–205.
7. Boman, H. G. (1995) Peptide antibiotics and their role in innate immunity. *Annu. Rev. Immunol. 13*, 61–92.
8. Raj, P. A., and Dentino, A. R. (2002) Current status of defensins and their role in innate and adaptive immunity. *FEMS Microbiol. Lett. 206*, 9–18.
9. Bauer, F., Schweimer, K., Kluver, E., Conejo-Garcia, J. R., Forssmann, W. G., Rosch, P., Adermann, K., and Sticht, H. (2001) Structure determination of human and murine β-defensins reveals structural conservation in the absence of significant sequence similarity. *Protein Sci. 10*, 2470–2479.
10. Kluver, E., Adermann, K., and Schulz, A. (2006) Synthesis and structure-activity relationship of β-defensins, multi-functional peptides of the immune system. *J. Pept. Sci. 12*, 243–257.
11. Kluver, E., Schulz-Maronde, S., Scheid, S., Meyer, B., Forssmann, W. G., and Adermann, K. (2005) Structure-activity relation of human β-defensin 3: Influence of disulfide bonds and cysteine substitution on antimicrobial activity and cytotoxicity. *Biochemistry 44*, 9804–9816.
12. Liu, S., Zhou, L., Li, J., Suresh, A., Verma, C., Foo, Y. H., Yap, E. P., Tan, D. T., and Beuerman, R. W. (2008) Linear analogues of human β-defensin 3: Concepts for design of antimicrobial peptides with reduced cytotoxicity to mammalian cells. *ChemBioChem 9*, 964–973.
13. Papo, N., and Shai, Y. (2003) Can we predict biological activity of antimicrobial peptides from their interactions with model phospholipid membranes?. *Peptides 24*, 1693–1703.
14. Vaara, M. (1992) Agents that increase the permeability of the outer membrane. *Microbiol. Rev. 56*, 395–411.
15. Vaara, M. (1992) The outer membrane as the penetration barrier against mupirocin in Gram-negative enteric bacteria. *J. Antimicrob. Chemother. 29*, 221–222.
16. Yu, L., Ding, J. L., Ho, B., Feng, S., and Wohland, T. (2008) Investigation of the Mechanisms of Antimicrobial Peptides Interacting with Membranes by Fluorescence Correlation Spectroscop. *The Open Chemical Physics Journal 1*, 62–79.
17. Epand, R. F., Savage, P. B., and Epand, R. M. (2007) Bacterial lipid composition and the antimicrobial efficacy of cationic steroid compounds (Ceragenins). *Biochim. Biophys. Acta 1768*, 2500–2509.
18. Suresh, A., and Verma, C. (2006) Modelling study of dimerization in mammalian defensins. *BMC Bioinf. 7*, S17.
19. Parks, Q. M., and Hobden, J. A. (2005) Polyphosphate kinase 1 and the ocular virulence of *Pseudomonas aeruginosa*. *Invest. Ophthalmol. Visual Sci. 46*, 248–251.
20. Diebold, Y., Calonge, M., Enriquez de Salamanca, A., Callejo, S., Corrales, R. M., Saez, V., Siemasko, K. F., and Stern, M. E. (2003) Characterization of a spontaneously immortalized cell line (IOBA-NHC) from normal human conjunctiva. *Invest. Ophthalmol. Visual Sci. 44*, 4263–4274.
21. Ramamoorthy, A., Thennarasu, S., Tan, A., Gottipati, K., Sreekumar, S., Heyl, D. L., An, F. Y., and Shelburne, C. E. (2006) Deletion of all cysteines in tachyplesin I abolishes hemolytic activity and retains antimicrobial activity and lipopolysaccharide selective binding. *Biochemistry 45*, 6529–6540.
22. Whiles, J. A., Deems, R., Vold, R. R., and Dennis, E. A. (2002) Bicelles in structure-function studies of membrane-associated proteins. *Bioorg. Chem. 30*, 431–442.
23. Yamamoto, K., Soong, R., and Ramamoorthy, A. (2009) Comprehensive Analysis of Lipid Dynamics Variation with Lipid Composition and Hydration of Bicelles Using Nuclear Magnetic Resonance (NMR) Spectroscopy. *Langmuir 25*, 7010–7018.
24. Guntert, P. (2004) Automated NMR structure calculation with CYANA. *Methods Mol. Biol. 278*, 353–378.
25. Wang, J., Schnell, J. R., and Chou, J. J. (2004) Amantadine partition and localization in phospholipid membrane: A solution NMR study. *Biochem. Biophys. Res. Commun. 324*, 212–217.
26. Mu, Y. (2009) Dissociation Aided and Side Chain Sampling Enhanced Hamiltonian Replica Exchange. *J. Chem. Phys. 130*, 164107.
27. Kollman, P. A., Massova, I., Reyes, C., Kuhn, B., Huo, S., Chong, L., Lee, M., Lee, T., Duan, Y., Wang, W., Donini, O., Cieplak, P., Srinivasan, J., Case, D. A., and Cheatham, T. E.III (2000) Calculating structures and free energies of complex molecules: Combining molecular mechanics and continuum models. *Acc. Chem. Res. 33*, 889–897.
28. Tieleman, D. P., van der Spoel, D., and Berendsen, H. J. C. (2000) Molecular dynamics simulations of dodecylphosphocholine micelles at three different aggregate sizes: Micellar structure and chain relaxation. *J. Phys. Chem. B 104*, 6380–6388.

29. Tieleman, D. P., Marrink, S. J., and Berendsen, H. J. (1997) A computer perspective of membranes: Molecular dynamics studies of lipid bilayer systems. *Biochim. Biophys. Acta 1331*, 235–270.
30. Van Der Spoel, D., Lindahl, E., Hess, B., Groenhof, G., Mark, A. E., and Berendsen, H. J. (2005) GROMACS: Fast, flexible, and free. *J. Comput. Chem. 26*, 1701–1718.
31. Onufriev, A., Bashford, D., and Case, D. A. (2004) Exploring protein native states and large-scale conformational changes with a modified generalized born model. *Proteins 55*, 383–394.
32. Morris, K. F. J., and Johnson, C. S. Jr. (1994) Mobility ordered 2D-NMR spectroscopy. *J. Am. Chem. Soc. 114*, 776–777.
33. Schibli, D. J., Hunter, H. N., Aseyev, V., Starner, T. D., Wiencek, J. M., McCray, P. B., Tack, B. F., and Vogel, H. J. (2002) The Solution Structures of the Human β-Defensins Lead to a Better Understanding of the Potent Bactericidal Activity of HBD3 against *Staphylococcus aureus*. *J. Biol. Chem. 277*, 8279–8289.
34. Hoover, D. M., Wu, Z. B., Tucker, K., Lu, W. Y., and Lubkowski, J. (2003) Antimicrobial characterization of human β-defensin 3 derivatives. *Antimicrob. Agents Chemother. 47*, 2804–2809.
35. Kluver, E., Adermann, K., and Schulz, A. (2006) Synthesis and structure-activity relationship of β-defensins, multi-functional peptides of the immune system. *J. Pept. Sci. 12*, 243–257.
36. Kluver, E., Schulz-Maronde, S., Scheid, S., Meyer, B., Forssmann, W. G., and Adermann, K. (2005) Structure-activity relation of human-defensin 3: Influence of disulfide bonds and cysteine substitution on antimicrobial activity and cytotoxicity. *Biochemistry 44*, 9804–9816.
37. Krishnakumari, V., Singh, S., and Nagaraj, R. (2006) Antibacterial activities of synthetic peptides corresponding to the carboxy-terminal region of human β-defensins 1−3. *Peptides 27*, 2607–2613.
38. Mandal, M., and Nagaraj, R. (2002) Antibacterial activities and conformations of synthetic α-defensin HNP-1 and analogs with one, two and three disulfide bridges. *J. Pept. Res. 59*, 95–104.
39. Mandal, M., Jagannadham, M. V., and Nagaraj, R. (2002) Antibacterial activities and conformations of bovine β-defensin BNBD-12 and analogs: Structural and disulfide bridge requirements for activity. *Peptides 23*, 413–418.
40. Pazgier, M., Li, X., Lu, W., and Lubkowski, J. (2007) Human defensins: Synthesis and structural properties. *Curr. Pharm. Des. 13*, 3096–3118.
41. Sahl, H. G., Pag, U., Bonness, S., Wagner, S., Antcheva, N., and Tossi, A. (2005) Mammalian defensins: Structures and mechanism of antibiotic activity. *J. Leukocyte Biol. 77*, 466–475.
42. Wu, Z. B., Hoover, D. M., Yang, D., Boulegue, C., Santamaria, F., Oppenheim, J. J., Lubkowski, J., and Lu, W. Y. (2003) Engineering disulfide bridges to dissect antimicrobial and chemotactic activities of human β-defensin 3. *Proc. Natl. Acad. Sci. U.S.A. 100*, 8880–8885.
43. Zou, G. Z., de Leeuw, E., Li, C., Pazgier, M., Li, C. Q., Zeng, P. Y., Lu, W. Y., Lubkowski, J., and Lu, W. Y. (2007) Toward understanding the cationicity of defensins: Arg and Lys versus their noncoded analogs. *J. Biol. Chem. 282*, 19653–19665.
44. Powers, J. P., Tan, A., Ramamoorthy, A., and Hancock, R. E. (2005) Solution structure and interaction of the antimicrobial polyphemusins with lipid membranes. *Biochemistry 44*, 15504–15513.
45. Porcelli, F., Buck-Koehntop, B. A., Thennarasu, S., Ramamoorthy, A., and Veglia, G. (2006) Structures of the dimeric and monomeric variants of magainin antimicrobial peptides (MSI-78 and MSI-594) in micelles and bilayers, determined by NMR spectroscopy. *Biochemistry 45*, 5793–5799.
46. Prenner, E. J., Lewis, R., Kondejewski, L. H., Hodges, R. S., and McElhaney, R. N. (1999) Differential scanning calorimetric study of the effect of the antimicrobial peptide gramicidin S on the thermotropic phase behavior of phosphatidylcholine, phosphatidylethanolamine and phosphatidylglycerol lipid bilayer membranes. *Biochim. Biophys. Acta 1417*, 211–223.
47. Abraham, T., Lewis, R., Hodges, R. S., and McElhaney, R. N. (2005) Isothermal titration calorimetry studies of the binding of a rationally designed analogue of the antimicrobial peptide gramicidin S to phospholipid bilayer membranes. *Biochemistry 44*, 2103–2112.
48. Dathe, M., and Wieprecht, T. (1999) Structural features of helical antimicrobial peptides: Their potential to modulate activity on model membranes and biological cells. *Biochim. Biophys. Acta 1462*, 71–87.
49. Shai, Y. (2002) Mode of action of membrane active antimicrobial peptides. *Biopolymers 66*, 236–248.
50. Tossi, A., Sandri, L., and Giangaspero, A. (2000) Amphipathic, α-helical antimicrobial peptides. *Biopolymers 55*, 4–30.
51. Bommineni, Y. R., Dai, H. E., Gong, Y. X., Soulages, J. L., Fernando, S. C., DeSilva, U., Prakash, O., and Zhang, G. L. (2007) Fowlicidin-3 is an α-helical cationic host defense peptide with potent antibacterial and lipopolysaccharide-neutralizing activities. *FEBS J. 274*, 418–428.
52. Hallock, K. J., Lee, D. K., and Ramamoorthy, A. (2003) MSI-78, an analogue of the magainin antimicrobial peptides, disrupts lipid bilayer structure via positive curvature strain. *Biophys. J. 84*, 3052–3060.
53. Kolusheva, S., Lecht, S., Derazon, Y., Jelinek, R., and Lazarovici, P. (2008) Pardaxin, a fish toxin peptide interaction with a biomimetic phospholipid/polydiacetylene membrane assay. *Peptides 29*, 1620–1625.
54. Rapaport, D., Peled, R., Nir, S., and Shai, Y. (1996) Reversible surface aggregation in pore formation by pardaxin. *Biophys. J. 70*, 2502–2512.
55. Sass, V., Pag, U., Tossi, A., Bierbaum, G., and Sahl, H. G. (2008) Mode of action of human β-defensin 3 against *Staphylococcus aureus* and transcriptional analysis of responses to defensin challenge. *Int. J. Med. Microbiol. 298*, 619–633.
56. Epand, R. M., Rotem, S., Mor, A., Berno, B., and Epand, R. F. (2008) Bacterial membranes as predictors of antimicrobial potency. *J. Am. Chem. Soc. 130*, 14346–14352.
57. Koradi, R., Billeter, M., and Wuthrich, K. (1996) MOLMOL: A program for display and analysis of macromolecular structures. *J. Mol. Graphics 14*, 51–55, 29−32.